Two-dimensional dynamics of a trapped active Brownian particle in a shear flow

Yunyun Li,[1,2] Fabio Marchesoni,[1,3] Tanwi Debnath,[4] and Pulak K. Ghosh[5]
[1]*Center for Phononics and Thermal Energy Science, School of Physics Science and Engineering, Tongji University, Shanghai 200092, People's Republic of China*
[2]*Shanghai Key Laboratory of Special Artificial Microstructure Materials and Technology, School of Physics Science and Engineering, Tongji University, Shanghai 200092, People's Republic of China*
[3]*Dipartimento di Fisica, Università di Camerino, I-62032 Camerino, Italy*
[4]*Department of Chemistry, University of Calcutta, Kolkata 700009, India*
[5]*Department of Chemistry, Presidency University, Kolkata 700073, India*
(Received 22 September 2017; revised manuscript received 19 November 2017; published 26 December 2017)

We model the two-dimensional dynamics of a pointlike artificial microswimmer diffusing in a harmonic trap subject to the shear flow of a highly viscous medium. The particle is driven simultaneously by the linear restoring force of the trap, the drag force exerted by the flow, and the torque due to the shear gradient. For a Couette flow, elliptical orbits in the noiseless regime, and the correlation functions between the particle's displacements parallel and orthogonal to the flow are computed analytically. The effects of thermal fluctuations (translational) and self-propulsion fluctuations (angular) are treated separately. Finally, we discuss how to extend our approach to the diffusion of a microswimmer in a Poiseuille flow. These results provide an accurate reference solution to investigate, both numerically and experimentally, hydrodynamics corrections to the diffusion of active matter in confined geometries.

DOI: 10.1103/PhysRevE.96.062138

I. INTRODUCTION

Specially designed synthetic microparticles are capable of propelling themselves by harvesting kinetic energy from an active environment [1–3]. Unlike bacteria [4,5], self-propulsion of inorganic microswimmers is fueled by *external* nonequilibrium processes, like directional mechanical impulses from catalytic chemical reactions or self-phoresis by short-scale (electric [6], thermal [7], or chemical [8]) gradients generated by the particles themselves through some built-in functional asymmetry [9]. In a quiescent suspension fluid such "active" swimmers undergo time-correlated Brownian motion, also termed active Brownian motion.

In shear flows, effects due to the intrinsically hydrodynamic nature of Brownian motion [10] may become prominent [11,12]. This statement is all the more true when it comes to characterizing the diffusion of sheared active swimmers in confined geometries. The interplay of shear gradients and self-phoretic propulsion is a topic of current investigation [13], as it is expected to advance our understanding of the collective dynamics of active swimmers [14,15] and their diffusion along confining walls and other fixed obstacles [16,17]. Indeed, recent progresses in the optical-tweezer technology [18] made particle fluctuations at the mesoscale accessible to experimental observation [19].

In this paper we focus on the the dynamics of a single active swimmer subjected to either a linear shear flow (Couette flow) or to a planar Poiseuille flow at low Reynolds numbers. Moreover, we assume that the particle freely diffuses at a distance from any obstacle so as its hydrodynamic interactions with the flow boundaries can be neglected [20]. The stochastic motion of a free particle moving along the streamlines of a viscous sheared fluid and the motion of the same particle trapped in a harmonic well swept through by the shear flow are immediately related. Of course, from an experimental viewpoint trapped particles (e.g., in an optical tweezer) offer a way more convenient setup for an accurate statistical analysis of sheared Brownian motion. This strategy has been adopted recently by a number of authors to investigate the Brownian motion of both passive [11,12,21] and passive particles [22–24].

The present study should be regarded as a preliminary work in preparation for a full-scale investigation of the hydrodynamics of two or more closely confined active swimmers. Data from numerical simulations will be then compared with the corresponding analytical results in the absence of hydrodynamic effects reported here. Our investigation confirms that active microswimmers tend to perform closed orbits, which are perturbed not only by the ubiquitous thermal fluctuations already considered in Ref. [11], but also by angular fluctuations intrinsic to their self-propulsion mechanism. The effects of these two sources of noise on the diffusion of the trapped swimmers are clearly separable. Similarly to the regular Brownian particles (i.e., passive swimmers) investigated in Ref. [11], as a consequence of the torque exerted by the shear gradient on the self-propelled swimmers [25–28], the ensuing random trajectories follow (quasi-) elliptical paths inclined at an angle with respect to the flow. Another remarkable property of trapped active swimmers is the chiral nature of their motion, also controlled by the shear gradient, which reflects in the oscillating time dependence of the cross-correlations between the particle displacements parallel and orthogonal to the flow.

This paper is organized as follows. In Sec. II we extend the standard two-dimensional (2D) model for a pointlike active Brownian particle of the Janus type we already investigated recently [29,30]. Additional features are the linear restoring force modeling the harmonic trap, the drag force exerted by the flow, and, finally, the torque associated with the shear gradient (constant in the Couette flow, linearly dependent on the transverse coordinate in a Poiseuille flow). Restricting our discussion to a 2D model greatly simplifies our calculations without a substantial loss of generality. In Sec. III we first study the dynamics of a trapped Janus particle subject to a Couette

flow. We prove that, in the noiseless regime, its planar orbits are elliptical and rotated with respect to the flow (Sec. III A). We then characterize the stochastic dynamics of the trapped particle by investigating its probability density function (p.d.f.) and the time dependence of its correlation functions $C_{ij}(t) = \langle x_i(t)x_j(0)\rangle$, where $i,j = 1,2$ and $x_1 = x$ and $x_2 = y$ denote, respectively, the longitudinal and transversal coordinates of the Cartesian plane. This analysis has been carried out separately in the presence of either thermal noise (Sec. III B) or angular noise (Sec. III C) alone. The extension of our analysis to the Poiseuille flow is discussed in Sec. IV, where the outcome of numerical simulation is compared with approximate analytical predictions based on the exact results of Sec. III. Finally, in Sec. V we physically interpret the different effects of the two noise sources on the dynamics of the trapped active particle.

II. THE MODEL

As anticipated in the Introduction, to avoid unnecessary complications, we limit this report to the case of 2D flows and pointlike active Brownian particles. The extension of our conclusions to 3D flows and finite-size particles will be discussed in a forthcoming paper. The simplest active particle realized so far is the two-faced Janus particle [2]. "Artificial swimmers" of this class get a continuous push from the suspension fluid, which in the overdamped regime is well modeled by a single self-propulsion velocity vector, $\mathbf{v}_0$, with constant modulus v_0.

In the absence of shear, the direction of $\mathbf{v}_0$ varies randomly with time constant τ_ϕ, under the combined action of thermal noise and fluctuations intrinsic to the self-propulsion mechanism. A shear flow $\mathbf{u}_s(\mathbf{r})$ affects the dynamics of a pointlike particle of coordinates $\mathbf{r}$ by forcing its self-propulsion velocity to rotate under the action of the local torque $\Omega = -(1/2)\nabla \times \mathbf{u}_s$. As a consequence, the particle free trajectories tend to bend with curvature radius inverse proportional to Ω [31,32].

A particle trapped in a symmetric harmonic potential well centered at $\mathbf{r}_0$ is subjected to an additional linear restoring force, $-k(\mathbf{r} - \mathbf{r}_0)$, which confines its motion in the center of the trap. By employing an optical tweezer is thus possible to record the random motion of a trapped active particle over long observation time intervals and with high time resolution [19].

The 2D stochastic dynamics of a harmonically trapped active particle of the Janus type is thus modeled by the following set of Langevin equations [28–30]:

$$\begin{aligned} \dot{x} &= v_0 \cos\phi - kx + u_s(y) + \xi_x(t), \\ \dot{y} &= v_0 \sin\phi - k(y - y_0) + \xi_y(t), \\ \dot{\phi} &= \Omega(y) + \xi_\phi(t), \end{aligned} \tag{1}$$

where the particle's center of mass is confined to the plane (x,y), subject to equilibrium thermal fluctuations represented by the Gaussian noises $\xi_i(t)$ with $\langle \xi_i(t)\rangle = 0$ and $\langle \xi_i(t)\xi_j(0)\rangle = 2D_0\delta_{ij}\delta(t)$ for $i = x,y$. The assumption that for $i \neq j$ $\langle \xi_i(t)\xi_j(0)\rangle = 0$ is surely correct in a quiescent suspension fluid where orthogonal fluctuations are separable but has been challenged in a shear flow. Thermal noise cross-correlations, if any, are small [33,34] and, therefore, can be safely ignored in this presentation.

The flow is directed along the x axis with shear gradient oriented along the y axis and the shear torque, $\Omega(y) = -(1/2)\dot{u}_s(y)$, orthogonal to the diffusion plane. The orientation of the self-propulsion velocity, ϕ, is given with respect to flow direction; see Fig. 1(b). The sign of Ω determines the positive (levogyre) or negative (dextrogyre) chirality of the particle. The fluctuations of the propulsion velocity are modeled here by the Gaussian noise $\xi_\phi(t)$ with $\langle \xi_\phi(t)\rangle = 0$ and $\langle \xi_\phi(t)\xi_\phi(0)\rangle = 2D_\phi\delta(t)$, where $D_\phi = 1/\tau_\phi$. In the bulk, self-propulsion contributes an additional amount $D_s = v_0^2/2D_\phi$ to the thermal diffusivity, D_0 [31,32]. We treated all noise sources in Eq. (1) as independently tunable, although, strictly speaking, thermal and orientational fluctuations may be statistically correlated [35]. More importantly, the parameters used in our simulations are experimentally accessible, as apparent on expressing times in seconds and lengths in micrometers (see Ref. [36] for a comparison).

We integrated numerically and, when possible, analytically the set of Langevin equations (1) for two types of stationary shear flows, both delimited by the symmetric planes $y = \pm y_L/2$, $-y_L/2 \leqslant y \leqslant y_L/2$, namely, the Couette flow

$$u_s(y) = -2u_0 y/y_L, \tag{2}$$

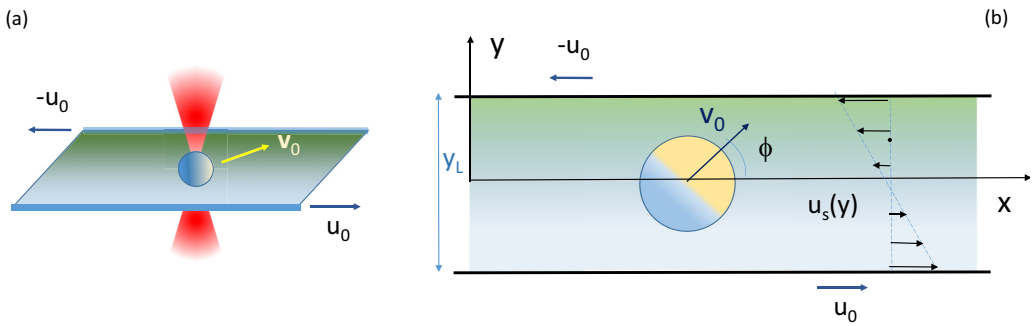

FIG. 1. Trapped Janus particle in a Couette flow: (a) ideal experimental setup. A Janus particle diffusing in a planar Couette cell is trapped by an optical tweezers directed orthogonally to the diffusion plane. $\mathbf{v}_0$ represents the instantaneous self-propulsion velocity, and $\pm u_0$ are the opposite speeds of the Couette cell walls. (b) Illustration of the 2D model of Eq. (1); see Sec. II.

with $\Omega = u_0/y_L$, and the planar Poiseuille flow,

$$u_s(y) = u_0[1 - (2y/y_L)^2], \tag{3}$$

with $\Omega(y) = 4u_0 y/y_L^2$.

The symmetric harmonic trap of elastic constant k was kept fixed at $\mathbf{r}_0 = (0, y_0)$. The choice of y_0 is irrelevant in the Couette flow (2), whereas it is expected to impact the particle's dynamics in the stationary Poiseuille flow (3) [25]. The numerical integration of the stochastic differential equations (1) was performed by means of a standard Euler-Maruyama scheme [37]. The stationary p.d.f.'s and the stochastic averages reported below were taken over ensembles of trajectories with random initial particle orientation, i.e., assuming a uniform ϕ distribution with $\phi(0) \in [0, 2\pi]$. Residual transient effects due to the choice of the injection coordinates, $x(0)$ and $y(0)$, were also discarded.

III. TRAPPING IN A COUETTE FLOW

We address first the simpler case of a harmonically trapped model Janus particle in the Couette flow of Eq. (2). The corresponding Langevin equations (1) boil down to a set of analytically tractable linear stochastic differential equations,

$$\begin{aligned} \dot{x} &= v_0 \cos\phi - kx - 2\Omega y + \xi_x(t), \\ \dot{y} &= v_0 \sin\phi - ky + \xi_y(t), \\ \dot{\phi} &= \Omega + \xi_\phi(t), \end{aligned} \tag{4}$$

where we set $y_0 = 0$ for convenience and made explicit use of the identity $u_s(y) = -2\Omega y$.

A. Noiseless regime, $D_0 = D_\phi = 0$

We start addressing the deterministic dynamics of a trapped Janus particle in the absence of fluctuation sources. Upon rescaling time, $t \to t' = kt$, one sees immediately that the particle's orbit depends on two parameters only, namely a length, v_0/k, which characterizes its size, and the dimensionless ratio shear torque to restoring force (in the overdamped limit), Ω/k.

The analytical integration of the equation set (4) with $D_0 = D_\phi = 0$ is a standard textbook exercise, which can be worked out in either the time or frequency domain. From the third equation (4), $\phi = \Omega t + \phi(0)$. Upon setting the time origin at $\phi(0) = 0$ and neglecting the exponentially decaying time transients that bear memory of the initial conditions of $x(t)$ and $y(t)$, one gets the following expressions for $x(t)$:

$$x(t) = A\ \cos(\Omega t + \alpha), \tag{5}$$

with $A = (v_0/k)\sqrt{1 + 9\Omega^2/k^2}/(1 + \Omega^2/k^2)$ and $\tan\alpha = (\Omega/k)(1 - 3\Omega^2/k^2)/(1 + 5\Omega^2/k^2)$, and for $y(t)$,

$$y(t) = B\ \sin(\Omega t + \beta), \tag{6}$$

with $B = (v_0/k)/\sqrt{1 + \Omega^2/k^2}$ and $\tan\beta = -\Omega/k$, which hold asymptotically in time, i.e., for $kt \gg 1$ and $\Omega t \gg 1$.

Having discarded all transients, Eqs. (5) and (6) provide a convenient parametric representation of the particle's orbit. The orbits plotted in Fig. 2 for different values of the model parameters exhibit a few interesting features:

(i) All orbits are closed and independent of the initial conditions. In this regard, we refer to them as limit cycles; see Fig. 2(a). They are quadrics centered at the origin:

$$\frac{x^2}{A^2} + \frac{y^2}{B^2} + 2\,\frac{xy}{AB}\sin(\alpha - \beta) = \cos^2(\alpha - \beta). \tag{7}$$

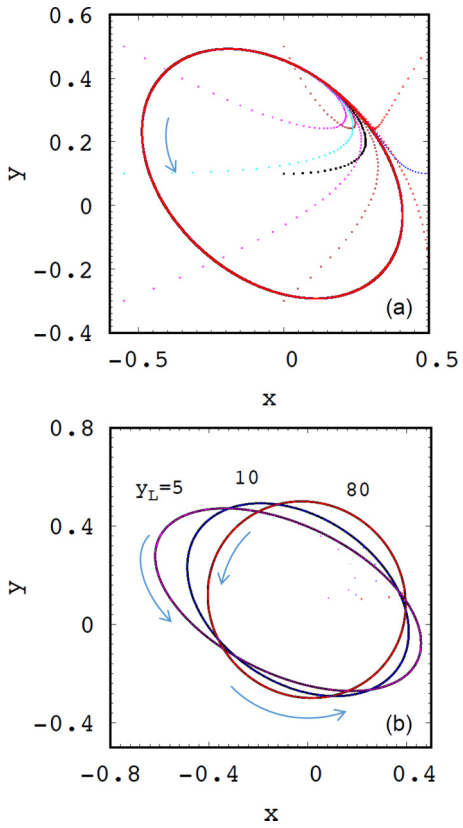

FIG. 2. Trapped Janus particle in the Couette flow of Eq. (2): noiseless regime. Plots have been produced by integrating Eqs. (4) for $D_0 = D_\phi = 0$, $v_0 = 1$, $k = 0.5$, $u_0 = 1$, and different y_L or $\Omega = u_0/y_L$ (see legends). (a) $y_L = 10$, limit cycle independent of the initial conditions, $x(0)$, $y(0)$, and $\phi(0)$. (b) Closed orbits for different Ω. For large t, the data points rest on the relevant orbits of Eq. (7).

(ii) Such orbits are ellipses with rotated axes [38], as one can easily conclude by inspecting Eq. (7). Their eccentricity increases with increasing Ω, whereas for vanishingly small torques one recovers a circle of radius v_0/k, as expected. For exceeding large Ω values both orbits' axes eventually shrink. The angle between the ellipse's major axis and the flow direction, Φ_e, is negative for $\Omega > 0$. From the analytical expression of Eq. (7),

$$\tan\Phi_e = -\frac{K}{1 + \sqrt{1 + K^2}}, \tag{8}$$

with $K = 2AB\sin(\alpha - \beta)/(A^2 - B^2)$. One notices immediately that the dependence of Φ_e on the torque is monotonic with $\Phi_e \to 0-$ for $\Omega/k \to 0$ and $\Phi_e \to -\pi/4+$ for $\Omega/k \to \infty$.

(iii) The limit cycle representations of Eqs. (5) and (6) and of Eq. (7) are validated in Fig. 2(b) by numerical integration of the deterministic model equations (4).

The tilted elliptical limit cycles of Fig. 2 are the result of a twofold action exerted by the shear gradient on the trapped active particle. For $\Omega > 0$ (positive chirality), the particle tends to move counterclockwise following a circular path. However,

in the upper (lower) branch of its orbit, as it moves from right (left) to left (right), it is subjected to an additional negative (positive) shear drag, $u_s(y) < 0$ $[u_s(y) > 0]$. This has the effect of distorting its circular path into an elliptical one with major axis rotated by the negative angle, $\Phi_e < 0$, of Eq. (8).

B. Thermal noise, $D_0 > 0$, $D_\phi = 0$

We next switch on the translational noises $\xi_x(t)$ and $\xi_y(t)$, while keeping $\xi_\phi(t) = 0$. By introducing dimensionless units, $t \to t' = kt$, $x \to x' = x/\sqrt{D_0/k}$ and $y \to y' = y/\sqrt{D_0/k}$, one notices that the dynamics of the trapped particle is now controlled by the ratio Ω/k, as before, and the ratio v_0^2/kD_0, which measures self-propulsion against thermal diffusion in the trap.

The calculation of all four correlation functions $C_{ij}(t)$ in the time domain is straightforward. From the second Langevin equation (4) we obtain the *asymptotic* solution

$$y(t) \equiv y^{(0)}(t) + y^D(t) = y^{(0)}(t) + e^{-kt}\int_{-\infty}^{t} e^{ks}\xi_y(s)\,ds, \tag{9}$$

where $y^{(0)}(t)$ is the deterministic solution of Eq. (6). The subtracted autocorrelation function of $y(t)$,

$$\begin{aligned} C_{yy}^{(s)}(t) &= C_{yy}(t) - C_{yy}^{(0)}(t) \\ &= \lim_{\tau\to\infty}[\langle y(t+\tau)y(\tau)\rangle - \langle y^{(0)}(t+\tau)y^{(0)}(\tau)\rangle_0] \\ &= \frac{D_0}{k}e^{-k|t|}, \end{aligned} \tag{10}$$

follows suite from the identity $\langle \xi_y(t)\xi_y(0)\rangle = 2D_0\delta(t)$. Here $C_{yy}^{(0)}(t)$ denotes the phase-averaged deterministic autocorrelation function $C_{yy}^{(0)}(t) = \langle y^{(0)}(t)y^{(0)}(0)\rangle_0 = (B^2/2)\cos\Omega t$; see Eq. (6).

The asymptotic solution for $x(t)$ depends on $y(t)$. On integrating the first Langevin equation (4), we derive a slightly more complicated, but still manageable expression for $x(t)$,

$$x(t) = x^{(0)}(t) + e^{-kt}\int_{-\infty}^{t} e^{ks}[-2\Omega y^D(s) + \xi_y(s)]\,ds, \tag{11}$$

with $x^{(0)}(t)$ given in Eq. (5). Contrary to $C_{yy}^{(s)}(t)$, the subtracted autocorrelation for $x(t)$ depends on the shear torque:

$$\begin{aligned} C_{xx}^{(s)}(t) &= C_{xx}(t) - C_{xx}^{(0)}(t) \\ &= \lim_{\tau\to\infty}[\langle x(t+\tau)x(\tau)\rangle - \langle x^{(0)}(t+\tau)x^{(0)}(\tau)\rangle_0] \\ &= \frac{D_0}{k}e^{-k|t|}\left[1 + 2\frac{\Omega^2}{k^2}(1+k|t|)\right]. \end{aligned} \tag{12}$$

In the derivation of Eq. (12) we made use of the following identities: $\langle \xi_x(t)\xi_x(0)\rangle = 2D_0\delta(t)$, $\langle y^D(t)\xi_x(0)\rangle = 0$ and $\langle y^D(t)y^D(0)\rangle = C_{yy}^{(s)}(t)$. The deterministic autocorrelation for $x(t)$, $C_{xx}^{(0)}(t)$, was calculated by averaging over the initial conditions, as done for $C_{yy}^{(0)}(t)$, hence, $C_{xx}^{(0)}(t) = \langle x^{(0)}(t)x^{(0)}(0)\rangle_0 = (A^2/2)\cos\Omega t$.

Finally, on combining solutions (11) and (9) for $x(t)$ and $y(t)$, respectively, and noticing that $\langle \xi_x(t)\xi_y(0)\rangle = \langle y^{(0)}(t)y^{(0)}(0)\rangle_0 = 0$, we calculate the cross-correlation functions

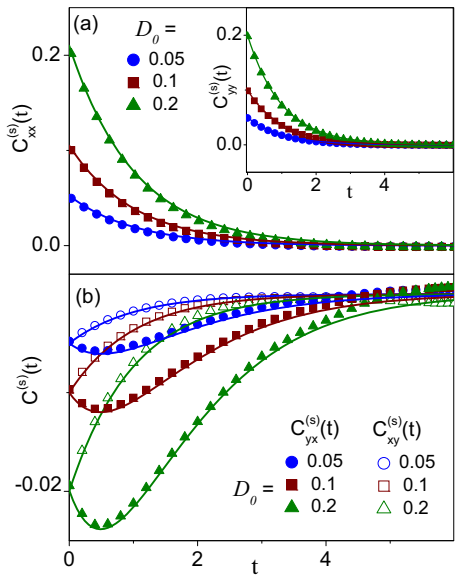

FIG. 3. Trapped Janus particle in the Couette flow, Eq. (2), with thermal noise. The subtracted auto- and cross-correlation functions have been computed by integrating Eqs. (4) for $D_\phi = 0$, $v_0 = 1$, $k = 1$, $u_0 = 1$, $y_L = 10$, and different D_0 (see legends). The solid curves represent the corresponding analytical predictions of Eqs. (10) and (12)–(14).

$$\begin{aligned} C_{xy}(t) &= \lim_{\tau\to\infty}[\langle x(t+\tau)y(\tau)\rangle \\ &= -\frac{D_0}{k}\frac{\Omega}{k}e^{-k|t|}[1 + 2kt\Theta(t)], \end{aligned} \tag{13}$$

$$C_{yx}(t) = C_{xy}(-t), \tag{14}$$

where $\Theta(\ldots)$ is the Heaviside function. Here $C_{xy}^{(0)}(t) = \langle x^{(0)}(t)y^{(0)}(0)\rangle_0 = 0$, so that the cross-correlations need not be subtracted, namely, $C_{xy}^{(s)}(t) = C_{xy}(t)$ and $C_{yx}^{(s)}(t) = C_{yx}(t)$.

The correlation function plotted in Fig. 3 have been obtained by numerical integration of Eqs. (4) for increasing levels of the thermal noise. The simulation points are closely fitted by the relevant curves of Eqs. (10) and (12)–(14). Moreover, one can easily check that our subtracted correlation functions coincide with the corresponding correlation functions obtained by the authors of Ref. [11] for a trapped passive particle (i.e., a simple colloidal particle) in a Couette flow. This suggests the conclusion, illustrated in Fig. 4, that the dynamics of a trapped active particle in a Couette flow can be separated into a deterministic chiral component, represented by its orbital motion along a limit cycle, an a stochastic perturbation, to be interpreted as the thermal fluctuations of the center of the limit cycle around the trap's bottom.

The separation of these two dynamical contributions is apparent in Fig. 4 at low thermal noise. The contours of the plotted 2D p.d.f.'s, $P(x,y)$, retain the shape of the limit cycle with $D_0 = 0$. Such an annular structure disappears only when D_0 is raised above a certain threshold, $\bar{D}_0$. An estimate for $\bar{D}_0$ is obtained by equating the free mean square displacement a passive particle undergoes in a time interval of the order of the

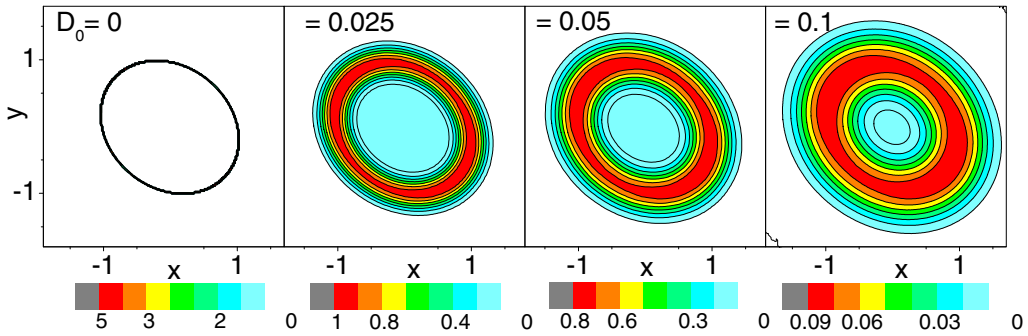

FIG. 4. Trapped Janus particle in the Couette flow, Eq. (2), with thermal noise. The contour plots of the p.d.f.'s $P(x,y)$ have been computed by integrating Eqs. (4) for $D_\phi = 0$, $v_0 = 1$, $k = 1$, $u_0 = 1$, $y_L = 10$ and increasing levels of translational noise (see legends). Note that the color scale changes from panel to panel.

trap's relaxation time, D_0/k, and the size squared of its limit cycle, $(v_0/k)^2$, that is, $v_0^2/k\tilde{D} \sim 1$. This argument justifies the physical interpretation of the ratio v_0^2/kD_0 given at the top of this section.

C. Angular noise, $D_0 = 0$, $D_\phi > 0$

Finally, we investigate the role of the angular noise, $\xi_\phi(t)$, on the orbiting motion of the harmonically trapped active particle. As done in Sec. III B, we first determine the minimal set of control parameters by introducing dimensionless units, that is, $t \to t' = kt$, $x \to x' = x/(v_0/k)$, and $y \to y' = y/(v_0/k)$. The ensuing free dynamical parameters are Ω/k, as in Sec. III B, and the ratio, D_ϕ/k, of the relaxation time in the trap, $1/k$, to the persistence time of the active Brownian motion, $\tau_\phi = 1/D_\phi$. v_0/k plays the role of a scalable length unit.

To calculate the four correlation functions $C_{ij}(t)$ we prefer to work here in the frequency domain. By taking the Fourier transform of both sides of the second equation (4) with $D_0 = 0$ and, then, calculating the square of their moduli, we obtain

$$S_{yy}(\omega) = \frac{v_0^2}{k^2+\omega^2}\, S_{cc}(\omega), \tag{15}$$

where $S_{yy}(\omega)$ and $S_{cc}(\omega)$ are, respectively, the Fourier transform of the stationary autocorrelation functions $C_{yy}(t)$ and $C_{cc}(t) = \langle \cos\phi(t)\cos\phi(0)\rangle$. Substituting $\phi(t) = \Omega t + \int_0^t \xi_\phi(s)ds$ in the latter and taking the stochastic average yield [35]

$$C_{cc}(t) = \frac{1}{2}\cos(\Omega t)e^{-D_\phi|t|}. \tag{16}$$

The inverse Fourier transform of Eq. (15) can be easily performed by applying the convolution theorem and making use of Eq. (16) for $C_{cc}(t)$. A lengthy calculation leads to the final result,

$$\begin{aligned} C_{yy}(t) = {} & \frac{v_0^2/2k^2}{\left(\Omega^2/k^2 + D_\phi^2/k^2 + 1\right)^2 - 4D_\phi^2/k^2} \\ & \times \left[\frac{D_\phi}{k}\left(\frac{\Omega^2}{k^2} + \frac{D_\phi^2}{k^2} - 1\right)e^{-k|t|} + 2\frac{D_\phi}{k}\frac{\Omega}{k}\sin(\Omega|t|)\right. \\ & \left. \times\, e^{-D_\phi|t|} + \left(\frac{\Omega^2}{k^2} - \frac{D_\phi^2}{k^2} + 1\right)\cos(\Omega t)e^{-D_\phi|t|}\right]. \end{aligned} \tag{17}$$

Two limits of Eq. (17) are worth mentioning:

(i) For $D_\phi \to \infty$, $C_{yy}(t) = (D_s/k)e^{-k|t|}$ with $D_s = v_0^2/2D_\phi$. As anticipated in Sec. II, in this limit the active particle behaves like a regular Brownian particle fluctuating in the trap with effective diffusion constant D_s.

(ii) For $D_\phi \to 0$, $C_{yy}(t) = v_0^2/[2(k^2+\Omega^2)]\cos\Omega t$, which is the autocorrelation function corresponding to the deterministic solution in Eq. (10).

The same procedure can be applied to the first Langevin equation (4) to calculate $C_{xx}(t)$. Making use of Eq. (15) we obtain the identity

$$S_{xx}(\omega) = \left(1 + \frac{4\Omega^2}{k^2+\omega^2}\right)S_{yy}(\omega) - \frac{4\Omega v_0^2}{k^2+\omega^2}\frac{S_{sc}(\omega)}{k+i\omega}, \tag{18}$$

where $S_{xx}(\omega)$ is the Fourier transform of $C_{xx}(t)$ and $S_{sc}(\omega) = S_{cs}^*(\omega)$ are the Fourier transforms of $C_{sc}(t) = \langle \sin\phi(t)\cos\phi(0)\rangle$ and $C_{cs}(t) = \langle \cos\phi(t)\sin\phi(0)\rangle$, respectively, with

$$C_{sc}(t) = C_{cs}(-t) = \tfrac{1}{2}\sin(\Omega t)e^{-D_\phi|t|}.$$

The explicit expression for the inverse Fourier transform of $S_{xx}(\omega)$ is cumbersome and thus of little use. The implicit expression in terms of $C_{yy}(t)$ and $C_{cs}(t)$,

$$\begin{aligned} C_{xx}(t) = {} & C_{yy}(t) + \frac{2\Omega^2}{k}\int_{-\infty}^{\infty} C_{yy}(s)e^{-k|t-s|}\,ds \\ & - \frac{2\Omega v_0^2}{k}\int_{-\infty}^{\infty} e^{-k|t-s|}\,ds\int_0^\infty e^{-ks'}C_{sc}(s-s')\,ds', \end{aligned} \tag{19}$$

can be used instead for practical purposes.

Finally, the Fourier transforms of $C_{xy}(t)$ and $C_{yx}(t)$ are also linear combinations of $S_{yy}(\omega)$ and $S_{cs}(\omega)$. For instance,

$$S_{xy}(\omega) = -\frac{2\Omega}{k+i\omega}\, S_{yy}(\omega) + \frac{v_0^2}{k^2+\omega^2}S_{cs}(\omega), \tag{20}$$

whence

$$\begin{aligned} C_{xy}(t) = {} & -2\Omega\int_0^\infty C_{yy}(t-s)e^{-ks}\,ds \\ & - \frac{v_0^2}{2k}\int_{-\infty}^{\infty} e^{-k|t-s|}C_{sc}(s)\,ds, \end{aligned} \tag{21}$$

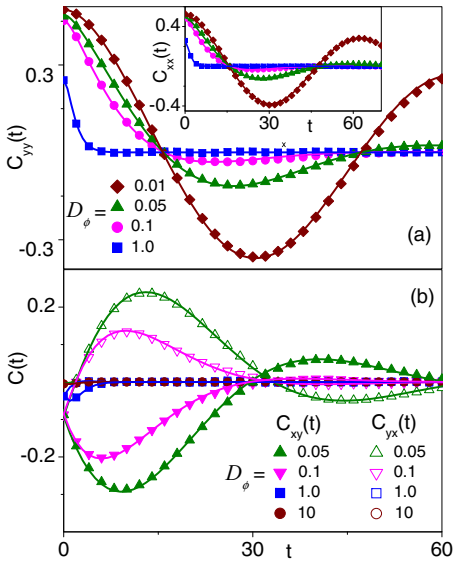

FIG. 5. Trapped Janus particle in the Couette flow, Eq. (2), with angular noise. The auto- and cross-correlation functions have been computed by integrating Eqs. (4) for $D_0 = 0$, $v_0 = 1$, $k = 1$, $u_0 = 1$, $y_L = 10$, and different D_ϕ (see legends). The dashed curves represent the corresponding analytical predictions of Eqs. (17) and (19)–(21).

and, similarly to Eq. (14),

$$C_{xy}(t) = C_{yx}(-t). \tag{22}$$

As a consistency test one can check that in the limit $D_\phi \to \infty$ Eqs. (21) and (22) coincide with Eqs. (14) and (13) after replacing D_0 by D_s. Moreover, all four correlation functions (17), (19), (21), and (22), fit pretty well the relevant data sets of Fig. 5, obtained by numerically integrating the model equations (4).

The 2D p.d.f.'s, $P(x,y)$, plotted in Fig. 6 for increasing D_ϕ values, well illustrate the effects of the angular noise on the motion of the trapped active particle. For $D_\phi = 0$ the particle follows its elliptical orbit with frequency Ω and orientation determined by the sign of Ω. Under the action of the angular noise, $D_\phi > 0$, the particle tends to randomly change direction on a time scale of the order of $\tau_\phi = 1/D_\phi$. In the regime $D_\phi \ll \Omega$, the particle retraces its limit circle repeatedly before leaving it. Vice versa, for $D_\phi \gg \Omega$ its trajectories tend to populate the region enclosed by the limit circle. In fact, as the confined particle orients its motion inward, it takes a time of the order of $(v_0/k)/v_0 = 1/k$ to reenter its deterministic orbit at some other point. It $\tau_\phi \gg 1/k$, that is $D_\phi \ll k$, the particle's trajectory will consist of extended arcs of the limit cycle. Correspondingly, in Fig. 6 the p.d.f.'s for $D_\phi \ll k$ exhibit a characteristic annular structure centered around the deterministic limit cycle, left panels, whereas for $D_\phi \gg k$, they tend to peak around its center, right panels.

IV. TRAPPING IN A POISEUILLE FLOW

The dynamics of an active particle of the Janus type harmonically trapped in the Poiseuille flow of Eq. (3) cannot be treated analytically because its shear torque is now a function of its distance, y, from the center of the flow, $\Omega(y) = 4u_0 y/y_L^2$. As a consequence, the model equations (1) turn nonlinear. We discuss here similarities and differences with the case of the Couette flow analyzed in Sec. III.

(i) Deterministic regime, $D_0 = D_\phi = 0$. Upon inserting Eq. (3) for $u_s(y)$ into the first Langevin equation (1), we first locate the effective trap center,

$$(x_c, y_c) = \left(\frac{u_0}{k}\left[1 - \left(\frac{2y_0}{y_L}\right)^2\right], y_0\right), \tag{23}$$

where y_0 is the transverse coordinate of the harmonic trap, while the longitudinal coordinate, x_0, was set to zero for convenience. The longitudinal shift of the trap's center, x_c, results from the equilibration between the flow drag, $u_s(y)$, and the harmonic restoring force, $-kx$.

Recalling that the linear dimensions of the orbit of a trapped active particle are of the order of v_0/k, we expect that for $|y_0 \pm y_L/2| \gg v_0/k$ in a Poiseuille flow a noiseless Janus particle moves along a closed orbit, not much differently than in the Couette flow of Sec. III A. For an appropriate choice of y_0 and v_0, the sign of $\Omega(y)$ is either definite positive for $v_0/k < y_0 < y_L/2 - v_0/k$, or definite negative for $-y_L/2 + v_0/k < -y_0 < -v_0/k$, which implies that the particle tends to orbit counter-clockwise or clockwise, respectively. The numerical integration of the model Eqs. (1) and (3) with $D_0 = D_\phi = 0$ supports this prediction; see Fig. 7(a). Furthermore, as in the Couette flow, the particle loses memory of its initial conditions after a transient time of the order of $1/k$ and eventually approaches a limit cycle.

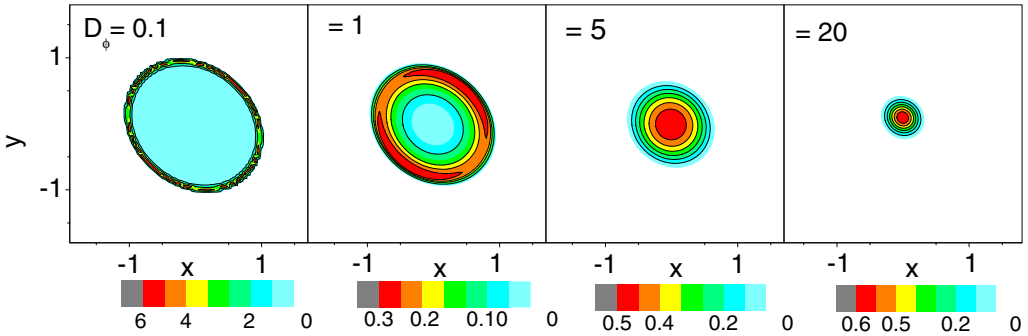

FIG. 6. Trapped Janus particle in the Couette flow, Eq. (2), with angular noise. The contour plots of the p.d.f.'s $P(x,y)$ have been computed by integrating Eqs. (4) for $D_0 = 0$, $v_0 = 1$, $k = 1$, $u_0 = 1$, $y_L = 10$, and different levels of the angular noise (see legend).

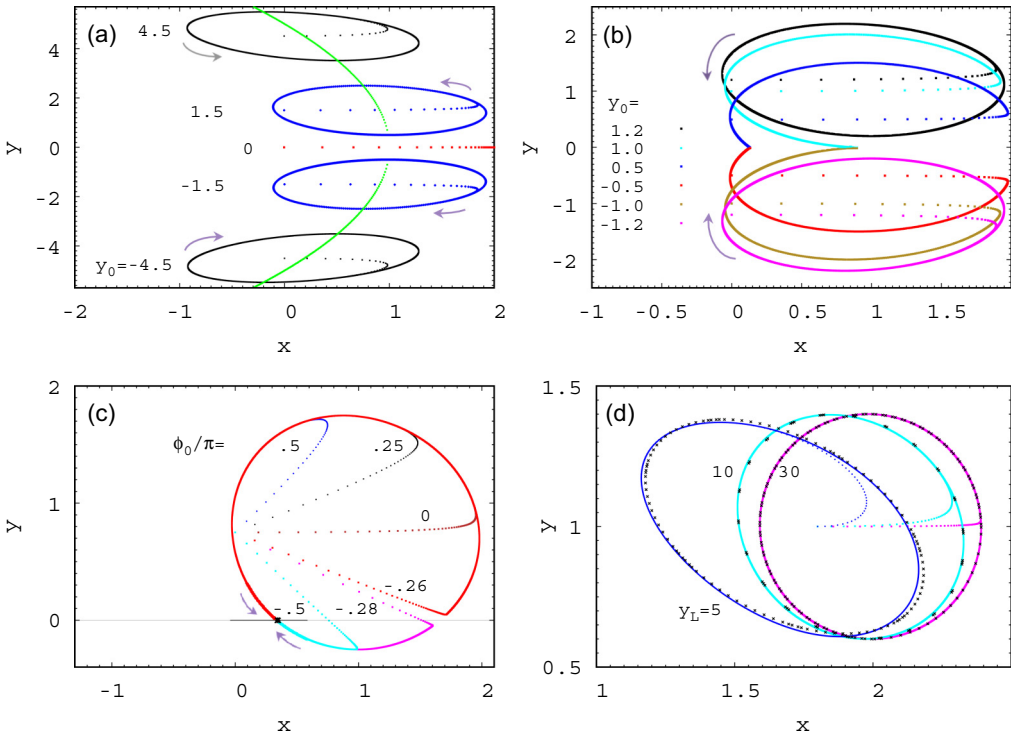

FIG. 7. Trapped Janus particle in the Poiseuille flow, Eq. (3): noiseless regime. Plots have been produced by integrating Eqs. (1) for $D_0 = D_\phi = 0$ and (a), (b) $v_0 = 1, k = 1, u_0 = 1\, y_L = 10$, and different y_0 (see legend); (c) $v_0 = 1, k = 1, u_0 = 1\, y_L = 10$, $y_0 = 0.75$ and different $\phi(0)$; (d) $v_0 = 0.2, k = 0.5, u_0 = 1\, y_0 = 1$, and different y_L (see legend). For all trajectories $x(0) = 0$ and $y(0) = y_0$. In panel (d) the approximate orbits of Eq. (24) are represented by crosses; the dotted parabola in panel (a) is the profile of the shear flow of Eq. (3) in arbitrary units.

An approximated analytical expression of such limit cycle for sufficiently large values of y_0 can be obtained by noticing that on increasing $|y_0|$ the fluid speed, $u_s(y)$, decreases, while the shear torque $\Omega(y)$ increases. As the angular frequency of the orbiting particle vanishes, setting $\dot{x} = \dot{y} = 0$ in Eqs. (1) yields

$$v_0^2 = [u_s(y) - kx]^2 + k^2(y - y_0)^2. \tag{24}$$

This simple formula fits quite closely the numerical limit cycles plotted in Fig. 7(d).

If the trap is placed closer to the flow centerline, $y = 0$, the orbiting particle may happen to cross it, which means that its shear torque, $\Omega(y)$, changes sign. Upon setting again $\dot{x} = \dot{y} = 0$ in Eqs. (1) and dropping the noise terms, one immediately recognizes that for $|y_0| < v_0/k$ there exists a fixed point solution (x_f, y_f) with

$$x_f = \frac{u_0}{k} - \sqrt{\left(\frac{v_0}{k}\right)^2 - y_0^2}, \quad y_f = 0, \tag{25}$$

where trajectories converge at an angle ϕ_f with respect to the flow, which must satisfy the geometric condition $\phi_f = -\arcsin(ky_0/v_0)$; see Figs. 7(b) and 7(c). The fixed point is always approached counterclockwise from above, $y \to 0+$ or $-\pi < \phi_f < 0$, and clockwise from below, $y \to 0-$ or $0 < \phi_f < \pi$, independently on the initial conditions. Moreover, depending on the initial conditions, the fixed point can be approached along two different paths (corresponding to different values of ϕ_f) for both $y \to 0+$ and $y \to 0-$. As shown in Fig. 7(c), in view of the system's mirror symmetry, each such path and the mirror image of the other one, joined together, form a closed orbit, also approximated by Eq. (24).

(ii) Stochastic dynamics. The noise effects on the dynamics of the trapped active particle is distinct in the presence of limit cycle or fixed point. As the noiseless self-propelled particle moves along a closed orbit [Fig. 7(a)] the action of thermal and angular noises can be well described by adapting the exact analytical results of Secs. III B and III C [11]. As a matter of fact, for $|y_0| \gg v_0/k$ we can expand $\Omega(y)$ in first order along the orbit's center (x_c, y_c), Eq. (23):

$$u_s(y) = u_s(y_0) + 2\Omega(y_0)(y - y_0).$$

Upon further translating the origin of the spatial coordinates to (x_c, y_c), $x \to x - x_c$ and $y \to y - y_c$, we reduce the set of nonlinear Langevin equations (1) to the set of linear ordinary stochastic equations introduced in Sec. III to model the dynamics of a harmonically trapped Janus particle in a Couette flow. As a consequence, for this range of model parameters, the analytical results of Sec. III apply to the Poiseuille flow, as well, with the only caution that the approximate shear torque, $\Omega(y_0)$, is now a function of the transverse coordinate of the trap, y_0. Accordingly, above (below) the flow centerline the particle tends to move counterclockwise (clockwise). This conclusion holds for both the correlation functions and the p.d.f.'s of the trapped active particle as confirmed by numerical simulation.

Switching on the noise terms when the noiseless dynamics of Eqs. (1) is governed by the fixed point of Eq. (25), (x_f, y_f), leads to a more peculiar stochastic dynamics. In Fig. 8(a) we plotted long trajectory samples of the same trapped active

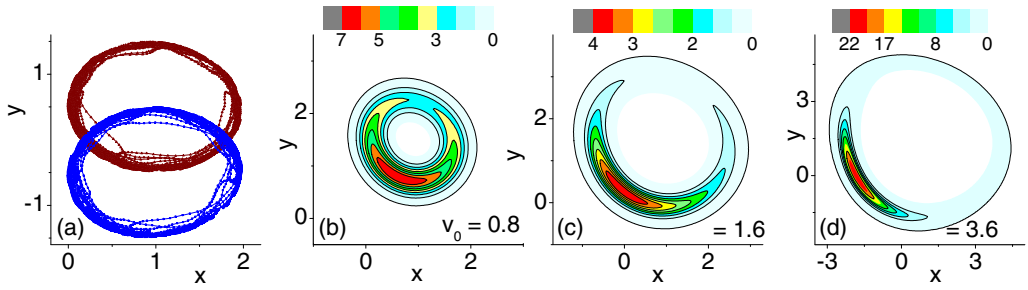

FIG. 8. Trapped Janus particle in the Poiseuille flow, Eq. (3): effect of noise around the flow centerline. Plots have been produced by integrating Eqs. (1) for $k = 1$, $u_0 = 1$, $y_L = 10$, and (a) $D_0 = 0$, $D_\phi = 0.1$, $v_0 = 1$, and $y_0 = \pm 0.5$ (upper/lower trajectory); (b)–(d) $D_0 = D_\phi = 0.025$, $y_0 = 1.5$, and different v_0 (see legend). Trajectories in (a) have been sampled over a time interval corresponding to 600 revolution periods $2\pi/\Omega(y_0)$. The contour plots of the 2D p.d.f. $P(x,y)$ in (b)–(d) help illustrate the particle's stochastic dynamics around the fixed point for $|y_0| < v_0/k$ (see text).

particle, but with opposite values of y_0. Contrary to the noiseless trajectories of Figs. 7(b) and 7(c), prodded by the angular noise, in both cases the particle seems to follow perturbed closed orbits passing in the vicinity of the fixed point. In the noiseless regime such orbits are mirror symmetric and, as illustrated in Fig. 7(c), consist each of two paths (one above and one below the flow centerline), which the particle traces with opposite orientations (counterclockwise and clockwise, respectively) as it approaches the fixed point. Accordingly, in the presence of noise, the particle does not run along an apparently closed orbit, as suggested by Fig. 8(a), but rather switches randomly between the two alternative paths that take it toward the fixed point. This interpretation is confirmed by the emergence of a prominent peak in the 2D p.d.f.'s plotted in Figs. 8(b)–8(d).

The $P(x,y)$ accumulation around (x_f, y_f) can be qualitatively explained by noticing that for an appropriate neighborhood of the fixed point $|\Omega(y)| \ll D_\phi$. Accordingly, the angular noise is more likely to kick the particle away from its deterministic path in that region of the plane, while the shear torque drives it back to it, following either deterministic paths as soon as $|\Omega(y)| \gg D_\phi$. In addition, the motion of the particle along the limit orbit is slower on the side closer to the shear centerline. For this reason the annular structures of the $P(x,y)$ in a Poiseuille flow are always biased toward the center of the flow.

V. CONCLUSIONS

We investigated the 2D dynamics of an active Brownian particle diffusing in a harmonic trap swept through a shear flow. Our work can be regarded as an extension of Ref. [11] with the key difference that the trapped colloidal particle considered here propels itself with constant speed and random orientation. Its dynamics is thus subjected to two distinct fluctuation sources, a 2D translational noise, due to the thermal fluctuations of the suspension fluid [11], and an angular noise, peculiar to the self-propulsion mechanism itself. As a noiseless 2D sheared active particle moves along a closed planar orbit, the translational noise sustains a harmonically confined Brownian motion of the orbit's center, while the angular noise makes the particle's trajectory diffuse around its deterministic orbit.

We analytically calculated the lower moments of the planar coordinates of the harmonically trapped active particle in a Couette flow; the exact results thus obtained were extended to investigate the richer diffusive dynamics that characterizes the very same bound system in a planar Poiseuille flow.

Our analysis was carried out under the assumptions that the active particle were isolated (that is away from the container walls and other swimmers, so as to ignore inevitable hydrodynamic effects) and the trap isotropic and harmonic. In a real optical tweezer the confining force is linear only close to the center, while nonconservative effects due to radiation pressure may arise in the outer region with a remarkable bias on particle's diffusion [39]. However, in the presence of appreciably strong self-propulsion, the resulting nonlinear contributions to the particle dynamics can be regarded as a next-to-leading correction to the model studied in the present work. More important are the effects due to the hydrodynamically mediated interactions among trapped active particles and between a trapped active particle and a fixed obstacle [16,17]. This is the subject of a forthcoming paper, where the outcome of extensive numerical simulations will be compared with the exact analytical results reported here.

ACKNOWLEDGMENTS

We thank RIKEN's RICC for computational resources. Y.L. is supported by the NSF China under Grant No. 11505128 and the Fundamental Research Funds for the Central University. P.K.G. was supported by a SERB Start-up Research Grant (Young Scientist) No. YSS/2014/000853 and the UGC-BSR Start-Up Grant No. F. 30-92/2015. T.D. thanks UGC, New Delhi, India, for the award of a Junior Research Fellowship.

[1] F. Schweitzer, *Brownian Agents and Active Particles* (Springer, Berlin, 2003).

[2] S. Jiang and S. Granick (eds.), *Janus Particle Synthesis, Self-assembly and Applications* (RSC Publishing, Cambridge, 2012).

[3] A. Walther and A. H. E. Müller, Janus particles: Synthesis, self-assembly, physical properties, and applications, Chem. Rev. **113**, 5194 (2013).
[4] M. J. McBride, Bacteria gliding motility: Multiple mechanisms for cell movement over surfaces, Annu. Rev. Microbiol. **55**, 49 (2001); H. C. Berg, *E. coli in Motion* (Springer, New York, 2013).
[5] J. Elgeti, R. G. Winkler, and G. Gompper, Physics of microswimmers, single particle motion and collective behavior: A review, Rep. Progr. Phys. **78**, 056601 (2015).
[6] S. Sengupta, M. E. Ibele, and A. Sen, Fantastic voyage: Designing self-powered nanorobots, Angew. Chem., Int. Ed. Engl. **51**, 8434 (2012).
[7] H. R. Jiang, N. Yoshinaga, and M. Sano, Active Motion of a Janus Particle by Self-Thermophoresis in a Defocused Laser Beam, Phys. Rev. Lett. **105**, 268302 (2010).
[8] Y. Hong, N. M. K. Blackman, N. D. Kopp, A. Sen, and D. Velegol, Chemotaxis of Nonbiological Colloidal Rods, Phys. Rev. Lett. **99**, 178103 (2007).
[9] R. Golestanian, T. B. Liverpool, and A. Adjari, Designing phoretic micro- and nano-swimmers, New J. Phys. **9**, 126 (2007).
[10] T. Franosch, M. Grimm, M. Belushkin, F. M. Mor, G. Foffi, L. Forró, and S. Jenney, Resonances arising from hydrodynamic memory in Brownian motion, Nature (London) **478**, 85 (2011).
[11] L. Holzer, J. Bammert, R. Rzehak, and W. Zimmermann, Dynamics of a trapped Brownian particle in shear flows, Phys. Rev. E **81**, 041124 (2010).
[12] H. Híjar, Harmonically bound Brownian motion in fluids under shear: Fokker-Planck and generalized Langevin descriptions, Phys. Rev. E **91**, 022139 (2015).
[13] For a review see A. Zöttl and H. Stark, Emergent behavior in active colloids, J. Phys.: Condens. Matter **28**, 253001 (2016).
[14] E. Lauga and T. R. Powers, The hydrodynamics of swimming microorganisms, Rep. Prog. Phys. **72**, 096601 (2009).
[15] M. C. Marchetti, J. F. Joanny, S. Ramaswamy, T. B. Liverpool, J. Prost, and M. Rao, Hydrodynamics of soft active matter, Rev. Mod. Phys. **85**, 1143 (2013).
[16] W. E. Uspal, H. Burak Eral, and P. S. Doyle, Engineering particle trajectories in microfluidic flows using particle shape, Nat. Commun. **4**, 2666 (2013).
[17] S. Das, A. Garg, A. I. Campbell, J. Howse, A. Sen, D. Valegol, R. Golestanian, and S. J. Ebbens, Boundaries can steer active Janus spheres, Nat. Commun. **6**, 8999 (2015).
[18] D. G. Grier, A revolution in optical manipulation, Nature (London) **424**, 810 (2003).
[19] S. Kheifets, A. Simha, K. Melin, T. Li, and M. G. Raizen, Observation of Brownian motion in liquids at short times: Instantaneous velocity and memory loss, Science **343**, 1943 (2014).
[20] C. Pozrikidis, *Fluid Dynamics*, 2nd ed. (Springer, New York, 2009).
[21] R. Mankin, K. Laas, and N. Lumi, Memory effects for a trapped Brownian particle in viscoelastic shear flows, Phys. Rev. E **88**, 042142 (2013).
[22] A. Nourhani, V. H. Crespi, and P. E. Lammert, Guiding Chiral Self-Propellers in a Periodic Potential, Phys. Rev. Lett. **115**, 118101 (2015).
[23] Y. Zong, J. Liu, R. Liu, H. Guo, M. Yang, Z. Li, and K. Chen, An optically driven bistable Janus rotor with patterned metal coatings, ACS Nano **9**, 10844 (2015).
[24] S. Jahanshahi, H. Löwen, and B. ten Hagen, Brownian motion of a circle swimmer in a harmonic trap, Phys. Rev. E **95**, 022606 (2017).
[25] A. Zöttl and H. Stark, Nonlinear Dynamics of a Microswimmer in Poiseuille Flow, Phys. Rev. Lett. **108**, 218104 (2012).
[26] T. Bickel, G. Zecua, and A. Würger, Polarization of active Janus particles, Phys. Rev. E **89**, 050303 (2014).
[27] J. Palacci, S. Sacanna, A. Abramian, J. Barral, K. Hanson, A. Y. Grosberg, D. J. Pine, and P. M. Chaikin, Artificial rheotaxis, Sci. Adv. **1**, e1400214 (2015).
[28] A. Geiseler, P. Hänggi, F. Marchesoni, C. Mulhern, and S. Savel'ev, Chemotaxis of artificial microswimmers in active density waves, Phys. Rev. E **94**, 012613 (2016).
[29] P. K. Ghosh, Y. Li, G. Marchegiani, and F. Marchesoni, Communication: Memory effects and active Brownian diffusion, J. Chem. Phys. **143**, 211101 (2015).
[30] D. Debnath, P. K. Ghosh, Y. Li, F. Marchesoni, and B. Li, Diffusion of eccentric microswimmers, Soft Matter **12**, 2017 (2016).
[31] S. van Teeffelen and H. Löwen, Dynamics of a Brownian circle swimmer, Phys. Rev. E **78**, 020101 (2008).
[32] For a minireview see X. Ao, P. K. Ghosh, Y. Li, G. Schmid, P. Hänggi, and F. Marchesoni, Active Brownian motion in a narrow channel, Eur. Phys. J. Spec. Top. **223**, 3227 (2014).
[33] K. Miyazaki and D. Bedeaux, Brownian motion in a fluid in simple shear flow, Physica A (Amsterdam) **217**, 53 (1995).
[34] B. Eckhardt and R. Pandit, Noise correlations in shear flows, Eur. Phys. J. B **33**, 373 (2003).
[35] P. K. Ghosh, V. R. Misko, F. Marchesoni, and F. Nori, Self-Propelled Janus Particles in a Ratchet: Numerical Simulations, Phys. Rev. Lett. **110**, 268301 (2013).
[36] G. Volpe, I. Buttinoni, D. Vogt, H.-J. Kümmerer, and C. Bechinger, Microswimmers in patterned environments, Soft Matter **7**, 8810 (2011).
[37] P. E. Kloeden and E. Platen, *Numerical Solution of Stochastic Differential Equations* (Springer, New York, 1992).
[38] B. Spain, *Analytical Conics*, Dover Books on Mathematics (Dover Publications, New York, 2007).
[39] H. W. Moyses, R. O. Bauer, A. Y. Grosberg, and D. G. Grier, A perturbative theory for Brownian vortexes, Phys. Rev. E **91**, 062144 (2015).